NASA Technical Memorandum 79293

FLUTTER SPECTRAL MEASUREMENTS USING STATIONARY PRESSURE TRANSDUCERS

A. P. Kurkov
Lewis Research Center
Cleveland, Ohio

Prepared for the
Twenty-fifth Annual International Gas Turbine Conference
and the Twenty-second Annual Fluids Engineering Conference
sponsored by the American Society of Mechanical Engineers
New Orleans, Louisiana, March 9-13, 1980

FLUTTER SPECTRAL MEASUREMENTS USING STATIONARY PRESSURE TRANSDUCERS

A. P. Kurkov

NASA Lewis Research Center
Cleveland, Ohio 44135

E-237

ABSTRACT

Engine-order sampling was used to eliminate the integral harmonics from the flutter spectra corresponding to a case-mounted static pressure transducer. Using the optical displacement data, it was demonstrated that the blade-order sampling of pressure data may yield erroneous results due to the interference caused by blade vibration. Two methods are presented which effectively eliminate this interference yielding the blade-pressure-difference spectra. The phase difference between the differential-pressure and the displacement spectra was evaluated.

NOMENCLATURE

A	amplitude
D	displacement in time units or in 1E periods, E^{-1}
d	displacement (cm), d = D·U (Fig. 1)
E	engine order
j	imaginary unit
n	number of points for spectral analysis
N	nodal diameter
P	unsteady pressure
P	steady-state pressure
r	radial coordinate (Fig. 1)
T	sampling period
t	time
U	wheel speed
α	stagger angle (Fig. 1)
c	fraction defined in equation (9)
$\Delta\theta$	angular deformation (Fig. 1)
Φ	angular coordinate in rotating frame of reference
Φ_1	Φ for blade 1
φ	phase angle, equation (2)
ψ	phase angle, equations (7) and (8)
ω	circular frequency

Subscripts:

f	flutter
i	corresponds to i'th nodal diameter
L	left
P	pressure
R	right
r	rotational

Superscripts:

D	displacement
P	pressure

INTRODUCTION

The use of stationary displacement sensors and high-response aerodynamic instrumentation for the turbomachinery flutter investigation was recently documented [1,2]. The aerodynamic instrumentation included a blade-wake velocity transducer and case-mounted static pressure transducers, while the displacement instrumentation consisted of two fibre-optics probes that sensed the light reflected from the rotor blade tips.

The advantages of stationary sensors over rotor-mounted sensors were demonstrated in these references particularly well due to the mistuned character of flutter. While a stationary sensor scans all the blades at a given position, a rotor mounted sensor performs a point-measurement only for one blade. Large variations in blade to blade vibratory amplitude and phase were reported from these measurements.

Another advantage of these sensors is derived from the fact that the phase difference between blades in the rotating frame of reference translates into a frequency shift in the stationary reference frame. Thus, the presence of several aerodynamic modes corresponding to different interblade phase angles is evidenced in a spectrum of a stationary sensor as the presence of several frequencies. Expressed in engine orders, these frequencies are easily identifiable because of the common non-integrality.

While the pressure and the displacement sensors are similar in regard to these properties, it may be noted that the pressure sensors yield a continuous signal whereas the displacement measurement is essentially discrete. Because of the continuity property, the spectral analysis of the pressure data is more difficult. The method presented in [2] is only adequate in the region where spatial unsteady pressure gradients are small, typically at midchord position. At the leading edge, however, large spatial variation

in amplitude and phase occurs within the blade passage [3], implying a wide frequency bandwidth of the stationary pressure signal. Transformation from a stationary into a rotating frame of reference such as described in [2] becomes then impractical.

This paper describes the alternate sampling and analyses techniques designed to eliminate the shortcoming of the previous procedure. The pressure in each blade passage is sampled at the same position relative to the equilibrium blade position, as in [2] for the discrete blade displacement signals. This avoids the superposition involved in the transformation into a rotating frame of reference, but introduces another difficulty associated with the fact that blades are vibrating and not still.

To deal with this problem two schemes are presented which result in blade-pressure-difference spectra. One scheme relies on the differential-pressure sampling in the steep-pressure-gradient region of the blade passage, and the other relies on the sampling in the two adjacent regions where the gradients are very small.

The paper also includes the optical displacement data at two chordwise positions. These data were sufficient to define the motion at the blade leading edge. Phasing of the blade-pressure-difference spectra and the displacement spectra at the leading edge indicated to which extent each nodal diameter component is contributing to the instability.

In addition to the above blade-passage (or blade-order) sampling, the paper includes a discussion of engine-order sampling in conjunction with its applicability for the on-line flutter detection.

The detailed documentation of the test conditions, the flutter boundaries, and the flow conditions in the relative frame of reference is available in [4]. The test point discussed in this report is 125.

EXPERIMENTAL MEASUREMENTS

The location of the instrumentation ports for the two types of measurements analyzed in this paper is illustrated in Fig. 1. The blade position in this figure includes incremental changes caused by load and speed which were estimated from manufacturer's data. Static pressures at other chordwise positions were also available; however, the leading edge transducer illustrates best the sampling and analyses techniques described in this paper.

The displacement data were recorded on a multichannel direct-record type tape recorder at 304.8 cm/s (120 in/s). Another FM tape was then generated by replaying the original tape at 7.62 cm/s (30 in/s) and recording the data at 304.8 cm/s (120 in/s). The frequency bandwidths were 2 MHz on the direct-record and 80 KHz on the FM. The direct-record method was used for the original data recording in order to avoid the frequency limitation encountered on the FM recorder. The pressure data, however, were recorded directly on the FM recorder.

Subsequent data processing was performed on a software-based Fast Fourier Transform (FFT) analyzer equipped with dual magnetic disc drives. The magnetic discs were used for storage and subsequent reprocessing of digital data. This capability essentially eliminated the need for the large computer and the central data processing facility which were used in the previous [2] displacement-data analysis. For the pressure data, the mass data storage capability enabled the implementation of special sampling techniques. The effective digitizing rate was 2.09 MHz for the displacement data and 1.31 MHz for the pressure data. These rates were achieved by greatly reducing the speed of the FM tapes on playback.

ANALYSIS OF THE DISPLACEMENT DATA

As can be seen in Fig. 1, instantaneous blade-tip position measurements were made at two chordwise positions. In addition to these, two reference pulses were recorded, the 1E and the 38E pulse, which corresponded to the blade passing frequency. These reference signals were generated by two magnetic sensors located opposite the appropriate triggers which were mounted on the rotor shaft.

In [2] all four channels of data were digitized simultaneously and stored on magnetic tapes. The displacements were obtained by measuring the positions of the trailing edge pulses relative to the corresponding 38E reference pulses. The 1E reference pulse provided the orientation in the relative frame of reference. Prior to the spectral analysis, the displacements were referenced to their respective averages in order to eliminate fluctuations resulting from blade spacing non-uniformities.

In this paper the data were digitized using the FFT analyzer which was limited to two channels. Digitized were either two of the three channels comprising the two optical data channels and the 38E reference pulse. The 1E reference pulse was used to initialize the digitization and was not itself digitized. It should be noted that either reference pulse could be used to calculate the displacements. The 38E reference pulse has been used due to better signal quality. In other respects the analysis of optical data was the same as in [2].

Figures 2, 3(a) and 3(b) present the overall spectra corresponding to the trailing-edge sensor vs 38E signal (relative to which the displacements were computed), the midchord sensor vs 38E signal, and the trailing edge sensor vs midchord sensor. A special procedure was followed when these data were digitized in order to assure that the data acquisition was initiated with the identical 1E reference pulse. This procedure will be discussed later in conjunction with the phasing of pressure and displacement spectra. Because the blades were sampled successively during each revolution, the number of samples per revolution was 38, and the highest detectable frequency was, therefore, 19E. The number of data points used in the spectral analysis was 2048, which approximately corresponded to 53.9 revolutions. The flutter frequency obtained independently from strain-gage data was 8.45E. (All available strain-gage data exhibited the same flutter frequency.)

In Fig. 2 the frequencies corresponding to major peaks are nonintegral by the same amount as the flutter frequency, i.e., 0.45E. The nodal diameters corresponding to this fraction can be obtained by subtracting the flutter frequency in engine orders from each frequency associated with this fraction. The possible range for nodal diameters so obtained is -8 to 10. Beyond this range, the nodal diameters correspond to aliased frequencies which are associated with fraction 0.55E. The spectral peaks corresponding to these frequencies are very small.

The phase angles corresponding to major peaks (i.e., corresponding to dominant frequency lines associated with major peaks) in Figs. 2 and 3 are presented in Table 1. They were determined neglecting the slight misalignment of the optical ports relative to the blade chord (Fig. 1). Choosing the trailing-edge sensor as the base, this correction would amount to the addition of 11.7 degrees to the phase corresponding to the midchord sensor. Because the amplitudes corresponding to this sensor are considerably smaller than for the trailing-edge sensor, the correction for the phase corresponding to Fig. 3(b), in the last row of Table 1 would be considerably smaller.

Because the phase angles corresponding to a given frequency in Table 1 are close to each other, and the spectra in Figs. 2 and 3 are nearly similar, the blade motion can be described as a rotation about a single point.

Using Figs. 2 and 3, the approximation

$$d = D\cdot U \approx \frac{r\Delta\Theta}{\sin\varepsilon} \qquad (1)$$

and the geometry in Fig. 1, the rotational axis was located at about 44 percent of chord from the leading edge. It is also possible to express the units in Fig. 2 in terms of angular deformation. As noted in this figure one unit corresponds to 0.117 degrees.

As in [2], the individual blade spectra can be obtained by arranging sampled data in groups so that each group includes successive samples from a particular blade only. Because the sampling for each blade is 1E, the resulting spectra are folded into the range 0 to 1/2E. Figure 4 presents the flutter amplitudes and phase angles for each blade as derived from the trailing-edge sensor vs 38E pulse data corresponding to 64 revolutions. The phase angles were referenced to blade one phase angle.

ANALYSIS OF THE PRESSURE DATA

Engine Order Sampling

The pressure data discussed in this paper are derived from a single portion of the tape which was digitized and stored on two magnetic discs. Two channels of data were digitized, the pressure signal from the leading edge transducer and the 1E reference signal. There was a total of 66 engine revolutions stored on discs and on the average the number of points per channel per revolution was 10295. This provided sufficient accuracy (i.e. 1/[10295E]) to illustrate the different sampling methods presented in this paper.

The main advantage of the engine-order sampling is that it enables the elimination of the steady-state part of the pressure signal so that only the non-integral, flutter related spectral peaks remain.

For the spectral analysis presented in this section, Fig. 5, the pressure data were sampled 512 times per revolution and the total number of revolutions was 16. This gave a total of 8192 points which was the maximum number that could be processed on the FFT analyzer. The nonfluctuating part of the pressure signal was removed by computing the average pressure (over 16 revolutions) for each of the 512 points, and then subtracting this average from the corresponding instantaneous pressures.

Although there were only 16 revolutions included in the computation of each average, the removal of the engine-order peaks was fairly effective. The most visible 38E peak was reduced in amplitude by about a factor of 34. The aliasing frequency for the data presented in Fig. 5 was 256; however, the contribution to the power spectrum beyond 128E (Fig. 5(b)) was very small which insured against aliasing in the range from 0 to 128E (Fig. 5(a)).

There are two non-integral frequency families in Fig. 5 associated with fractions 0.45 and 0.55. The former is associated with nodal diameters greater than or equal to -8 and the latter with nodal diameters less than -8. This can be seen by expressing the spectral peaks in Fig. 5 as [2],

$$A_i\cos[\omega_r(N_i + \omega_f/\omega_r)t + \varphi_i] \qquad (2)$$

Because only positive frequencies can be detected by spectral analysis, for $N_i < -\omega_f/\omega_r$, the above expression takes the form,

$$A_i\cos[\omega_r(-N_i - \omega_f/\omega_r)t - \varphi_i] \qquad (3)$$

It is seen now that the flutter frequency expressed in engine orders is being subtracted from the positive whole number ($-N_i$) yielding the fraction 0.55. It is noted that the phase angle is reflected about the horizontal axis.

It can be shown that if all frequencies corresponding to the significant peaks in Fig. 5 were folded about the frequency multiples of 19E, as many times as necessary, so that they fall in the range of 0 to 19E, only the frequencies which are also present in Fig. 2 would remain. If pressure transducers were mounted on each blade, the nodal diameters corresponding to these frequencies would be the only ones detected, because in this case the measurement is spatially discrete. It follows therefore, that there are no new nodal diameters, or modes resulting from the spectral analysis of the pressure data. The apparent nodal diameters seen by the stationary pressure transducers are the result of a complex pressure distribution in the blade channels, the description of which requires a large number of spatial harmonics.

Although the spectral results such as in Fig. 5 are illustrative, for the purpose of quantitative analysis they are not very convenient. In order to obtain the nodal diameters, it is necessary to fold frequencies in Fig. 5, and in order to transform the results into a rotating frame of reference it is necessary to perform superposition [2]. Both require the knowledge of phase angles for all significant peaks in this figure. In view of their large number and a wide frequency spread, this is difficult to accomplish. The wide frequency spread also implies a limited accuracy due to the memory limitation of the spectral analyzer.

However, the spectral results such as in Fig. 5 can be used for the purpose of flutter detection. In this case, the engine-order sampling could be performed directly utilizing the device termed the angle clock (or angle encoder) [1] as the external sampler. The angle clock is essentially a frequency multiplier which is capable of generating an arbitrary number of pulses per revolution from an input 1E pulse. The accuracy of this device, which is now commercially available is comparable to that achieved presently through the use of the analog tape and peripheral digital storage devices. The removal of the non-fluctuating part of the pressure signal essentially involves the computation of the average which does not entail any appreciable time delay.

An additional advantage of the engine-order sampling is that for the undersampled data the folding occurs either about an integral frequency or an integral frequency plus 1/2E, depending on whether the number of points per revolution is even or odd. Therefore, by selecting an even number of points per revolution there would be only two fractions associated with a flutter frequency even for the aliased sampling. For the purpose of flutter detection, a more important consideration than the aliasing is that the total number of revolutions included in the sample be large, which facilitates the efficient removal of engine order peaks. As will be shown later, it is also desirable that the number of samples per revolution is not a multiple of the number of blades on the rotor.

Blade-Passage Sampling

In this section an alternate sampling and an analysis method for the pressure data is presented. The sampling is performed once per blade passage at the same position relative to the steady-state pressure distribution.

Prior to the sampling, therefore, the steady-state distribution had to be determined. This was achieved by separating the data recorded on discs into records covering the period of one revolution, as determined from the reference 1E pulse data. The points within each revolution were then ordered relative to the start of the revolution and the corresponding points in each record were averaged over a total number of revolutions. The resulting steady-state distribution consisted of 10295 points, each representing the average of 66 revolutions. Figure 6 illustrates a typical distribution for a blade passage with the right-hand gradient region presented enlarged. In this figure the horizontal axis is given in terms of number of digitized points relative to an arbitrary origin. The basic unit of time is therefore 1/(10295 E). The marked points in Fig. 6 subdivide the gradient region into equal parts each of which is seven spaces wide. These points represent the locations relative to the zero crossing where the pressure was sampled. The zero crossings themselves, being common to all points, were determined in advance and stored on a disc.

One important consideration for the sampling in the pressure-gradient region is the blade motion itself. In terms of units of Fig. 6 the blade displacement was about 5. Motion of this extent introduces a fluctuating pressure in addition to the fluctuations which would be recorded if the blades were not vibrating. It is possible to demonstrate this effect indirectly by showing that the vibratory motion - as derived from the pressure data in the gradient region - does not compare well with the vibratory motion derived from the optical displacement data.

The blade vibration is reflected in the pressure data as a periodic displacement of the gradient portion of the pressure distribution relative to its equilibrium or steady-state distribution. The pressure data can, therefore, be processed quite similarly to the optical pulse data, the main difference being that the instantaneous blade position is obtained relative to the 1E reference pulse rather than relative to a corresponding 38E pulse. The spectral results obtained in such a way are presented in Fig. 7(a). If there were no interference from the pressure fluctuations, these results would be similar to the optical displacement spectrum in Fig. 2. The fact that they are different indicates that there is interference from pressure fluctuations. Superposition of two signals for an i'th nodal diameter can be expressed as

$$A_i^D \cos\left[(\omega_f + \omega_r N_i)t + \psi_i^D\right] + A_i^P\left(\frac{d\bar{P}}{dt}\right)^{-1} \cos\left[(\omega_f + \omega_r N_i)t + \psi_i^P\right] \quad (4)$$

where the superscripts D and P denote respectively displacements and pressures.

This unconventional analysis of pressure data was specifically performed to illustrate the displacement signal contamination due to pressure fluctuations. The sampling was performed at a constant pressure level corresponding to point 7 in Fig. 6. More conventional results in Fig. 7(b), however, were obtained by reversing this process, i.e., by sampling pressures at the position defined by this point. It is seen that results in these two figures are quite similar. Both represent the summation of two signals, one derived from the pressure fluctuation and the other from the blade motion as shown in equation (4). Corresponding expression for Fig. 7(b) would differ only by a multiplicative factor $d\bar{P}/dt$. It would illustrate contamination of pressure fluctuations due to blade vibratory motion.

Gradient Sampling

One solution to this problem is to form a pressure difference in the region where the steady-state pressure gradient is approximately constant. Because the blade displacement is the same on both sides of the blade, and the gradient is approximately constant, the contribution to the pressure difference from the blade motion is nearly cancelled.

To illustrate this, pressures were sampled at indicated points in Fig. 6 and then the following differences were formed, $P_7 - P_0$, $P_{14} - P_7$, $P_{14} - P_0$ and $P_{21} - P_{-7}$. The spectra corresponding to these differences are given in Fig. 8 and phase angles are presented in Table 2. The number of sampled data points used for spectral analysis was 2048. Because the pressures in each difference above were not sampled at the same time, a more exact procedure would be to obtain transforms for each point individually, apply the appropriate correction to the phase angle of one point and then perform the subtraction in the frequency domain. However, the maximum correction for the phase angle for the results presented in Fig. 8 would be 8 degrees. Therefore, the results obtained using the latter procedure would not differ appreciably from the above.

It can be seen that the pressure-difference spectra in Fig. 8 are all qualitatively similar and that they are similar to the displacement spectrum in Fig. 2. Comparison of the amplitudes of corresponding peaks in Fig. 8 also indicates that in the approximately constant-gradient region between points 0 and 14 (Fig. 6) the amplitudes are approximately proportional to the number of intervals between the pair of points included in the difference. If this interval is maintained constant the exact position of the pair of points does not seem to be important. Comparison of phase angles at a given frequency in Table 2 indicates that they are nearly constant.

These observations can be explained qualitatively based on physical arguments. Because it takes a finite time to traverse the static pressure port and because of the finite blade thickness in the direction of the wheel speed, it is expected that the pressure difference across the blade will be smeared over approximately 10 points. This corresponds approximately to half the width of the steep gradient region in Fig. 6. It appears, therefore, that the smearing of the pressure difference is in part due to dimensional effects.

Considering first the smearing due to static port dimensions only, one can treat the blade as a discontinuity as shown in Fig. 9. The sketch on the left corresponds to the left-point gradient sampling and on the right to the right-point gradient sampling (Fig. 6). The instantaneous blade position is defined in terms of the area fraction f, where $f = 0$ corresponds to the position of the blade when it is aligned with the left edge of the port. Subscripts L and R denote left and right positions, and P and S denote the blade pressure and suction sides. The pressure difference between the right and left pressures is then

$$P_R - P_L = f_R P_P + (1 - f_R)P_S - [f_L P_P + (1 - f_L)P_S]$$

or,

$$P_R - P_L = (f_L - f_R)(P_S - P_P) \quad (5)$$

Since all pressures are vectors, possessing amplitude and phase, and f is real, it follows that the pressure difference between the two points in the constant-gradient region has the same phase as the suction-pressure side difference. It can also be seen that the proportionality of amplitude and the distance between the two points should hold approximately in the central region where fraction f is approximately proportional to the blade position.

Using two approximations, an explanation could also be offered for the case of finite blade thickness and negligible pressure-port dimensions. The first is the quasi steady-state assumption, based on the fact that the blade thickness is small compared to the wavelength corresponding to one flutter cycle, and the second is the linearity of pressure variation in the tip-clearance region over the blade thickness.

Zero Gradient Sampling

Because the interference with pressure fluctuations due to blade motion is proportional to the steady-state pressure gradient, an alternate way of eliminating this interference is to sample in the region where pressure gradients are small, or ideally, zero. For example, Fig. 10(a) presents the spectrum for point - 14 (Fig. 6) which is still fairly close to the steep gradient region of the pressure distribution. It can be seen that this spectrum is qualitatively much closer to the displacement spectrum in Fig. 2 than the one in Fig. 7(b), which was obtained by sampling in the steep gradient portion of the blade passage.

In order to obtain the pressure difference across the blade, one also has to select a point in the zero slope region on the suction side of the blade. Because of considerable curvature in the steady-state pressure distribution in this region and the blade to blade differences, this is more difficult. Based on results obtained so far, one would expect that the spectrum for this point should also be qualitatively similar to the displacement spectrum in Fig. 2. It was found that this condition is reasonably satisfied for point 28 (Fig. 6). The spectrum for this point is presented in Fig. 10(b), the pressure difference spectrum corresponding to points 28 and -14 in Fig. 10(c), and its phase in Table 2. The spectral amplitude and phase for the pressure difference $P_{28} - P_{-14}$ is seen to be close to the respective values obtained for $P_{21} - P_{-7}$.

Although it has not been stated explicitly thus far, the underlying assumption for obtaining a valid pressure difference across the blade is that the pressure variation over an interval corresponding to the distance between the two points selected for computation of the difference should be small, except when crossing the blade. One way to check this assumption is to form a pressure difference in the approximately flat region to the left of the zero crossing in Fig. 6, e.g., $P_{-7} - P_{-14}$. It is not likely that these two points will bracket the blade and therefore one should expect amplitudes which are much smaller than a difference involving the same number of points in the gradient region. This is substantiated by comparing results in Figs. 10(d), 8(a) and 8(b) corresponding respectively to $P_{-7} - P_{-14}$, $P_7 - P_0$ and $P_{14} - P_7$ difference.

Smearing Effects Due to Blade Motion

In a previous section the pressure-difference smearing due to the finite dimensions of the transducer and the blade was examined. However, even in the absence of dimensional effects, in the gradient region some smearing can also occur due to the blade motion. Because the two sampling positions for the pressure-difference spectra were selected based on the average pressure distribution, and because of blade vibratory motion, it is possible to have both pressure samples forming a difference on the same side of the blade at least sometimes. This would tend to reduce the magnitude of the pressure difference.

To simulate this effect, two data sets are utilized associated respectively with the spectra in Figs. 10(d) and 8(d). The first set, corresponding to Fig. 10(d) is representative of the pressure difference when both pressures are on the same side of the blade and the second, corresponding to Fig. 8(d), is representative of pressure difference data when the two pressures forming the difference are on the opposite sides of the blade. A third data set was then created by random sampling of the first data set followed by substitution of the sampled values into corresponding points in the second set. Only points which have not been selected previously were substituted in the second set. In the particular case considered, the third data set consisted of 1024 points from the first and 1024 points from the second set. Spectral amplitudes for these data are presented in Fig. 11 and phase angles in Table 1. It can be seen that the spectral peaks are approximately proportional to the number of points from the data set corresponding to Fig. 8(d), and that phase angles agree fairly well with other corresponding phase angles in Table 1. Considering the magnitude of peaks in Fig. 11 one can associate this spectrum with the one in Fig. 8(c) which corresponds to the pressure difference $P_{14} - P_0$. Qualitatively, one of the principal differences between these two figures is the higher noise level in Fig. 11. However, this may be due to the fact that the pressure difference in Fig. 11 originates from two points which are apart twice the distance involved in Fig. 8(c). The larger distance between the points in Fig. 11 implies that the noise between these two points is less correlated and that, therefore, during subtraction the cancellation of noise is less pronounced.

CORRELATION OF PRESSURE AND DISPLACEMENTS

In order to be able to correlate the measurements recorded on different tapes it was essential to be able to initialize digitization at exactly the same time. This was achieved by using a time code reader which produced a pulse at the instant the continuously read time from the tape matched the preselected time dialed on the time code reader. The data acquisition was initiated at the first 1E reference pulse following this instant. The coincidence condition was detected under software control and the 1E reference pulse was used as the external trigger. The suggestion for the use of the time code reader and its implementation in this procedure was made by W. H. Jones of NASA Lewis.

Because the time code for the displacement data was not available on the original digital-record tape, it was not possible to correlate directly the pressure and displacement data. (An arbitrary referenced time code, however, was recorded on the FM copy of the displacement data tape enabling repeated replay of this tape at the identical 1E reference pulse). In order to correlate the displacement and the pressure data, it was necessary, therefore, to use the strain-gage data for which the time code was available. This was accomplished using a procedure which is best illustrated by reviewing the resulting expressions for the correlated displacement and pressure signals. For an arbitrary i-th nodal diameter these expressions are

$$P,D = \sum_{i=1}^{38} A_i^{P,D} \exp j\left[\omega t - (\Phi - \Phi_1)N_i + \psi_i^{P,D}\right] \qquad (6)$$

where P and D denote respectively pressure and displacement. Reference time t = 0 corresponds to the instant a particular 1E reference pulse reaches a predetermined level and, as indicated, the reference angle corresponds to blade 1 angular position. The phase angles ψ_i for the displacements and pressures are given respectively as

$$\psi_i^D = \varphi_i^D + \frac{37}{38} N_i 2\pi - \frac{0.455}{38} 2\pi \frac{\omega_f}{\omega_r} + \psi_1^S -$$

$$\tan^{-1} \frac{\sum A_i^D \sin\left(\varphi_i^D + \frac{37}{38} N_i 2\pi - \frac{0.455}{38} 2\pi \frac{\omega_f}{\omega_r}\right)}{\sum A_i^D \cos\left(\varphi_i^D + \frac{37}{38} N_i 2\pi - \frac{0.455}{38} 2\pi \frac{\omega_f}{\omega_r}\right)} \qquad (7)$$

$$\psi_i^P = \varphi_i^P + \frac{9}{38} N_i 2\pi - \frac{1}{38} 2\pi \frac{\omega_f}{\omega_r} \qquad (8)$$

In these expressions φ_i's are the i-th nodal diameter phase angles measured relative to the first point in the input data set for spectral analysis. For the displacement data, this point corresponded to the first blade that appeared under the sensor following the 1E trigger and for the pressure data it corresponded to the second blade after the 1E trigger. (The latter choice was necessary because the first blade under the sensor was slightly past the selected triggering level at the time of 1E trigger.) The second terms in these expressions account for the position of blade one relative to the above reference blades for φ_i's, and the third terms account for the time delay between the occurrence of the 1E pulse and the instance appropriate reference blades are under the respective sensors. The fourth term in the expression for ψ_i^D, φ_1^S is the phase angle for the blade-one above-shround-trailing-edge gage (ASTE gage [4]) relative to the 1E trigger, and the last term accounts for the arbitrary time reference for the displacement data. This term represents the phase of blade one at the time of 1E trigger. It was actually evaluated from the aliased 1/2E spectrum associated with this blade, and not from the given expression.

The strain-gage phase φ_1^S, was determined by interpolation between the frequency lines, similar as in [2]. However, a simpler and more accurate approximation was used for fraction ϵ which defines the true frequency relative to a neighboring frequency line. This approximation is due to D. Braun of NASA Lewis. If ω_f is the true frequency and the two most significant amplitudes are A_1 and A_2 corresponding to frequencies ω_1 and ω_2, and $\omega_1 < \omega_f < \omega_2$, then

$$\epsilon_1 = \frac{(\omega_f - \omega_1)nT}{2\pi} \sim \frac{A_2}{A_1 + A_2} \qquad (9)$$

The phase angle corresponding to ω_f is equal to the phase angle at ω_1 minus $\epsilon_1\pi(n-1)/n \sim \epsilon_1\pi$. In practice, the accuracy with which ϵ_1 can be determined is usually limited by the signal to noise ratio. An estimate on the accuracy can therefore be made using this ratio. Another estimate on the accuracy may be obtained by varying parameters in the spectral analysis. Sampling in the range of about 8 to about 32 points per cycle, a spread in the phase angle φ_1^S of about 10 degrees was encountered. It is therefore estimated that this phase angle is accurate within ±5 degrees.

Because of the availability of the Singleton FFT-algorithm [5], the spectral analysis of the displacement and pressure data discussed in this section was performed on a large computer. This algorithm does not require that the number of points for spectral analysis be a power of two. It is possible, therefore, to select the size of the input data block for the spectral analysis consisting of an integral number of revolutions and having approximately an integral number of cycles. This results in a uniform nonintegrality of flutter peaks and minimizes the fraction ϵ_1 (computed relative to the frequency line corresponding to the dominant peak).

For the displacement data, the number of data points was 2470, corresponding to 65 revolutions and containing 549.1 flutter cycles (associated with $N_i = 0$). For the pressure data, the number of data points corresponded to 63 revolutions, and the number of flutter cycles was 523.9. Different choice for the number of revolutions for the pressure data was governed by a slight shift in the flutter frequency expressed in engine orders.

The phase angles corresponding to different peaks in the respective spectra were obtained by using an effective fraction ϵ. For the displacement phase angles, it was obtained by averaging the ϵ's corresponding to six most significant peaks, and for the pressure phase angles, it was obtained by averaging values corresponding to two most significant peaks. The phase angles were estimated to be accurate within about ±10 degrees.

The phase difference between pressure and displacement vectors is presented in Table 3. Because pressure leads the displacement, all modes in this table are unstable.

It is noted that precise determination of the moment coefficient and the work per cycle would require a repeated application of the methods outlined in this paper at the remaining chordwise locations. However, because the unsteady force on the blade during stall flutter is concentrated near the leading edge [3,6], the conclusion regarding the stability of different modes reached in this paper is not expected to change by this extension.

DISCUSSION OF RESULTS

In reviewing the different method of analysis of pressure data presented in this paper, it may be noted that basic to all is the engine-order sampling followed by the removal of the steady-state part of the pressure signal at each sampled point. If pressure signals are processed mainly for flutter detection, as already mentioned, it is desirable that the number of samples per revolution be not an integral multiple of the number of blades. This assures that pressures at different relative positions in the blade passage are sampled so that the possibility of sampling only in a region where the unsteady pressure signal is small, or perhaps not even detectable, is eliminated. For example, sampling once per blade passage at a point located at 110 intervals relative to the zero crossing (Fig. 6) results in a spectrum with 11.45 peak reduced by a factor of 4.6 and the 5.45 peak by a factor of 2.3 relative to the corresponding peaks in Fig. 10(b).

Blade-order sampling is therefore better suited for post-run data analysis when the precise blade-passage position of the sampled point can be controlled and the possible interference due to the steady-state pressure gradient taken into account.

Two methods are available to accomplish this, the gradient pressure-difference sampling and the zero-gradient sampling. The former method can only provide pressure-difference spectra while the latter also yields the pressure spectra close to the blade surfaces. In general, the applicability of each method will depend on the character of the steady-state distribution. In the particular case, the gradient method appears to be easier to apply. This method yields correct phase results, and the amplitudes are attenuated approximately as the ratio of the distance between the two points to the distance corresponding to the full extent of the gradient region.

It is noted that in the computation of the unsteady work per cycle, the interference due to the blade motion is of no consequence since it is either in or out of phase with the displacement so that it does not contribute to the work integrated over a flutter cycle.

The analysis of pressure data has been given thus far in terms of the over-all spectra. An analogous procedure would be to use the individual blade spectra, similarly to Fig. 3 for the displacements. Figure 12, for example, illustrates such results for the pressure difference $P_{21} - P_{47}$. Such results were also obtained for all points in Fig. 6 and all the differential pressures associated with these points. However, the over-all spectra, which exhibit system characteristics, were found to be more convenient to use for the analysis. Results such as in Fig. 12 lead to a discussion of the individual blade characteristics which appeared to be less consistent than the system as a whole.

CONCLUDING REMARKS

An analysis procedure based on engine-order sampling was presented which effectively eliminates the engine harmonics from the overall spectra corresponding to a stationary pressure transducer. It was shown how this procedure can be implemented for the on-line flutter detection.

Quantitative spectral analyses of pressure data were performed based on blade order sampling. Optical displacement spectra were used to demonstrate the interference of blade motion with the pressure signal in the steep gradient portion of the blade passage. Two methods were outlined which yield the blade-pressure-difference spectra removing the contribution due to the blade motion.

Phasing of the blade differential pressure and the displacement spectra at the leading edge indicated that pressure leads the displacement for the six most significant nodal-diameter modes.

REFERENCES

1 Nieberding, W. C. and Pollack, J. L., "Optical Detection of Blade Flutter," ASME Paper No. 77-GT-66, Mar. 1977.

2 Kurkov, A. and Dicus, J., "Synthesis of Blade Flutter Vibratory Patterns Using Stationary Transducers," ASME Paper No. 78-GT-160, Apr. 1978.

3 Stargardter, H., "Subsonic/Transonic Stall Flutter Study," Pratt & Whitney Aircraft, East Hartford, Conn., NASA Contract NAS3-20606.

4 Jeffers, J. D., May, A., and Deakin, W. J., "Evaluation of a Technique for Predicting Stall Flutter in Turbine Engines," PWA-FR-9620, Pratt & Whitney Aircraft, West Palm Beach, Fla., Feb. 1978. (NASA CR-135423)

5 Singleton, R. C., "On Computing the Fast Fourier Transform," Comm. ACM, Vol. 10, No. 10, Oct. 1967, pp. 647-654.

6 Carta, F. O. and St. Hilaire, A. O., "Effect of Interblade Phase Angle And Incidence Angle on Cascade Pitching Stability," ASME Paper No. 79-GT-153, Mar. 1979.

TABLE 1. - PHASE ANGLES, DISPLACEMENT SPECTRA

Figure	Frequency (E)						
	3.45	4.45	5.45	8.45	11.45	12.45	13.45
2	-65	-61	-57	48	-68	-68	-65
3(a)	-56	-54	-49	77	-83	-79	-86
3(b)	-66	-64	-59	46	-63	-65	-56

TABLE 2. - PHASE ANGLES, PRESSURE-DIFFERENCE SPECTRA

Figure	Frequency (E)						
	3.45	4.45	5.45	8.45	11.45	12.45	13.45
8(a)	-144	133	43	-132	-161	98	28
8(b)	-144	129	59	-134	-161	101	38
8(c)	-144	131	51	-133	-161	99	33
8(d)	-149	127	47	-132	-163	96	36
10(c)	-142	131	48	-136	-171	90	27
11	-133	128	48	-136	-164	95	35

TABLE 3. - DIFFERENTIAL-PRESSURE PHASE RELATIVE TO DISPLACEMENT PHASE

ΔP	Nodal diameter						
	-5	-4	-3	0	3	4	5
$P_{14} - P_0$	7	11	14	25	33	24	51

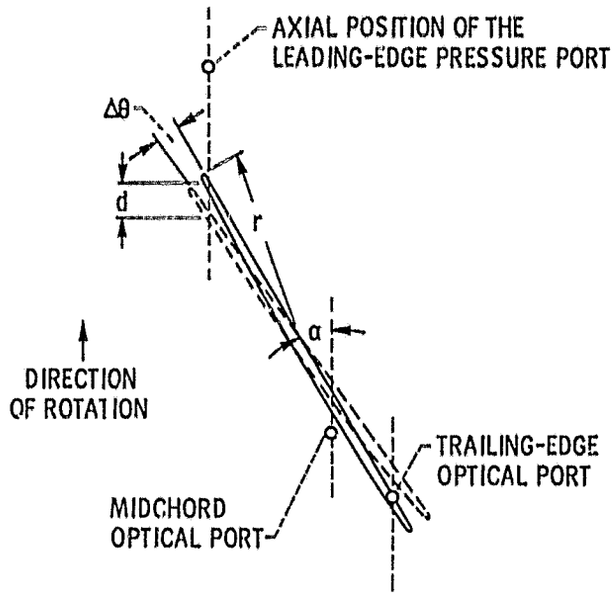

Figure 1. - Location of measurements ports.

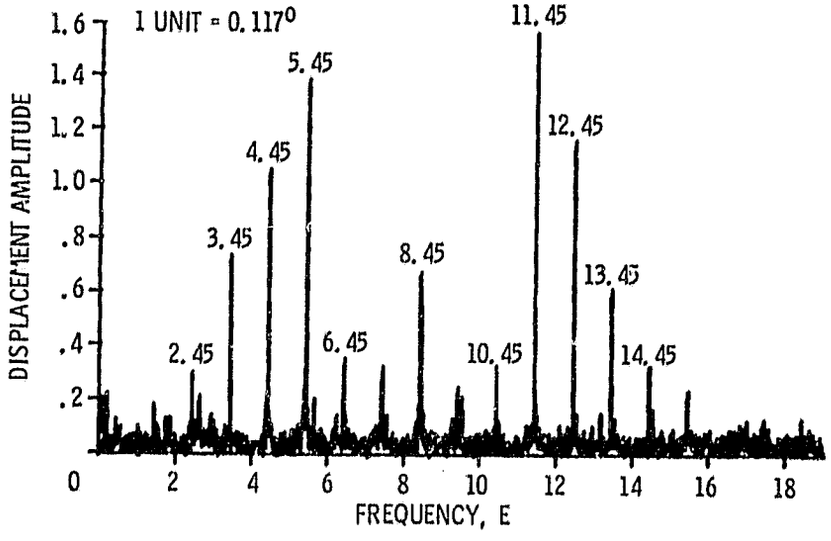

Figure 2. - Displacement-amplitude spectrum, trailing-edge sensor, 1 unit = 1/(16475 E).

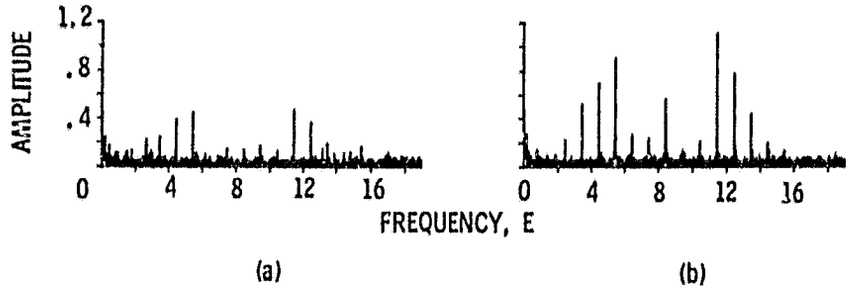

Figure 3. - Displacement spectra corresponding to the midchord (a), and the trailing-edge versus midchord sensor (b), 1 unit = 1/(16475 E).

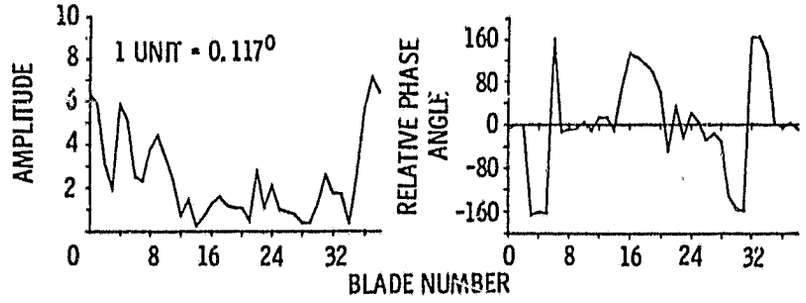

Figure 4. - Displacement amplitude and phase distribution.

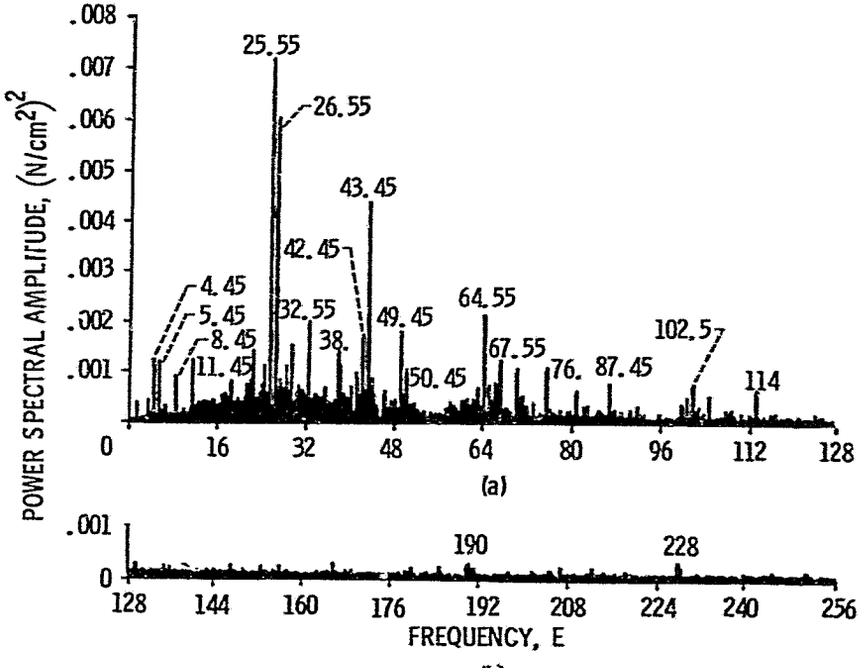

Figure 5. – Power spectrum of the leading-edge pressure transducer signal.

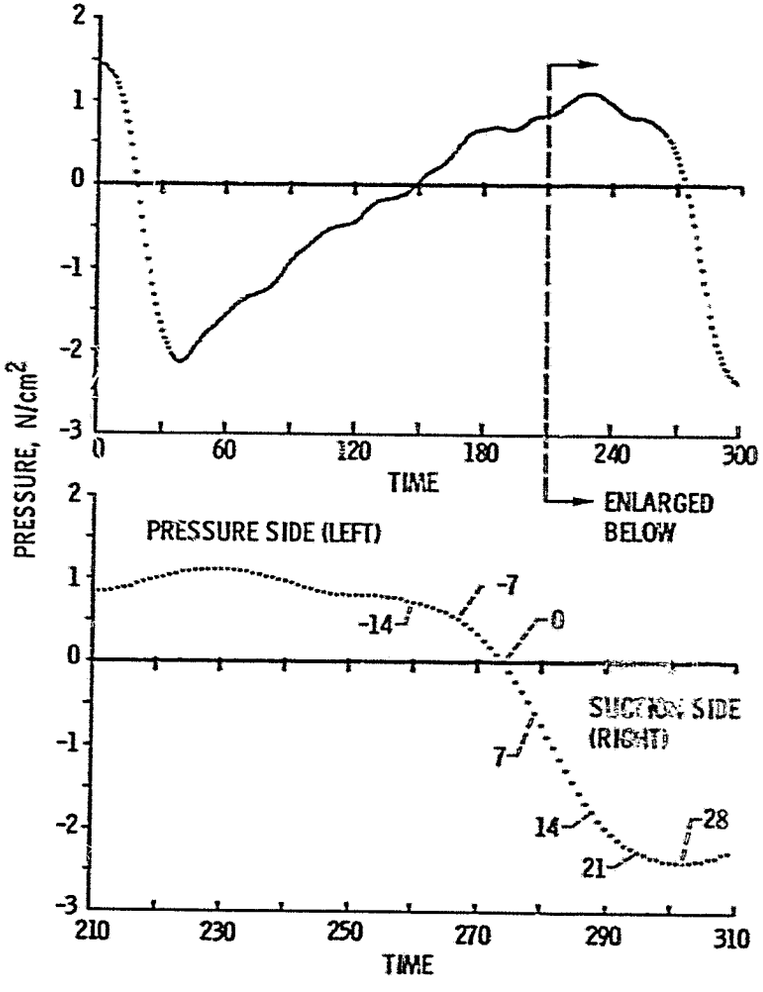

Figure 6. – Steady-state pressure distribution; 1 unit = 1/(10295 E).

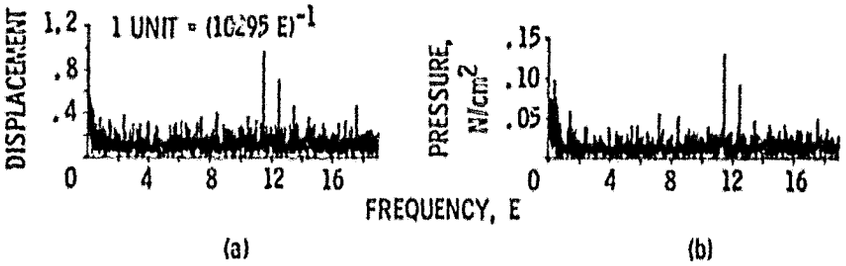

Figure 7. - Apparent displacement and pressure spectra as derived from pressure data by sampling in the steep gradient region.

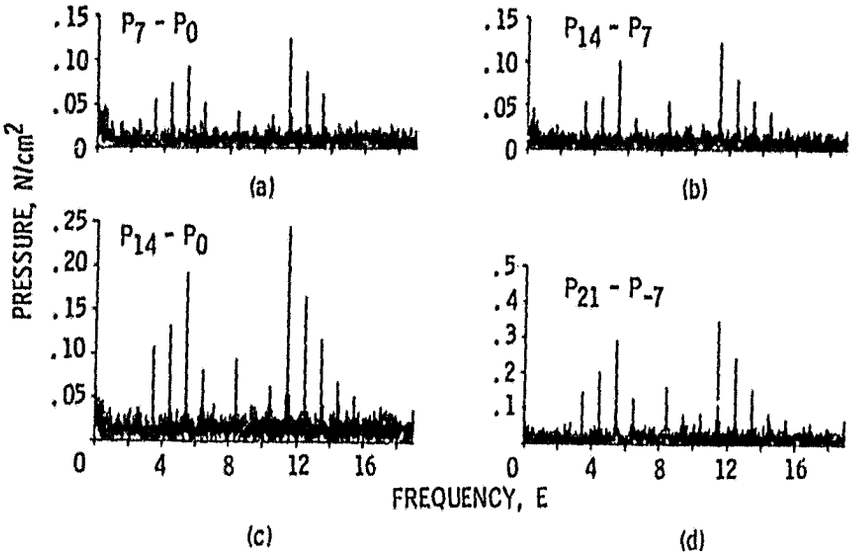

Figure 8. - Pressure-difference spectra, gradient sampling.

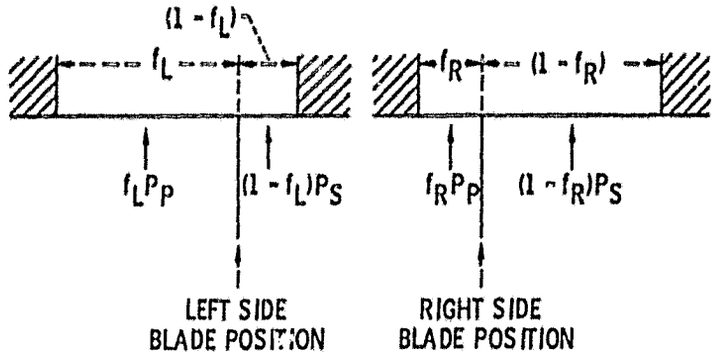

Figure 9. - Smearing effect due to the finite dimensions of the pressure port.

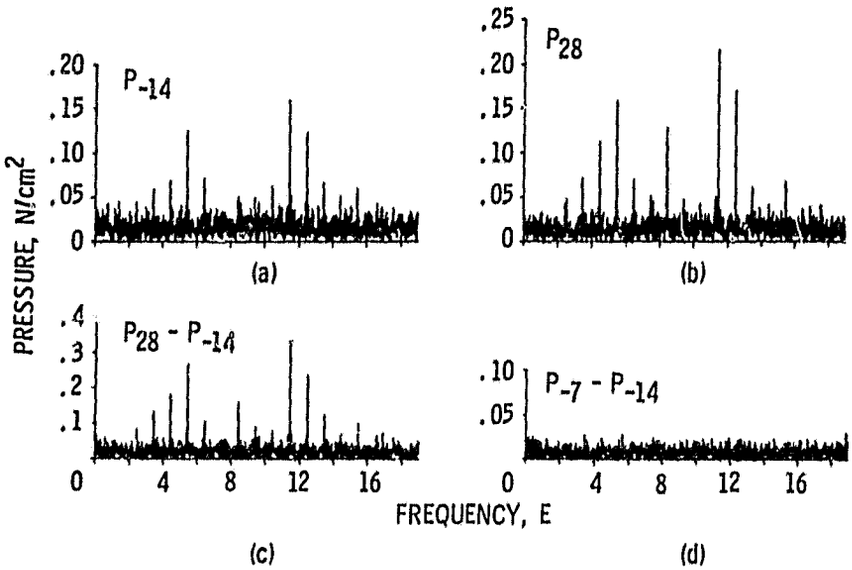

Figure 10. - Spectral results based on sampling outside of the steep-gradient region.

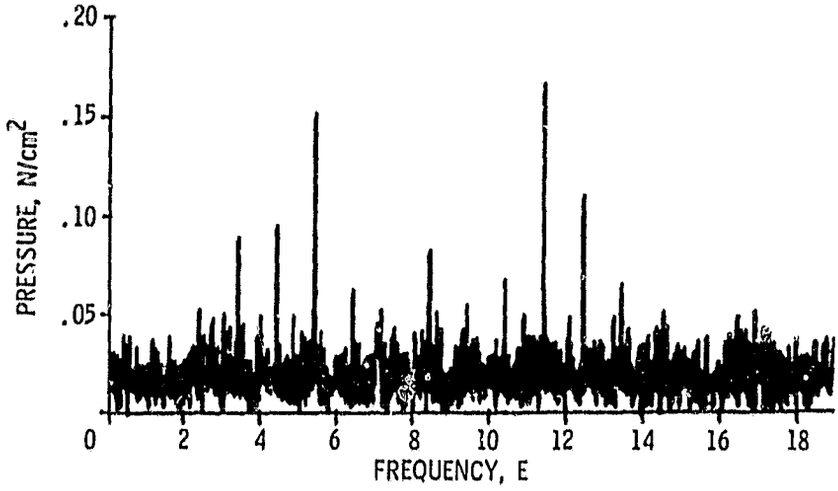

Figure 11. - Pressure spectrum derived from $P_{21} - P_{-7}$ and $P_{-7} - P_{-14}$ data sets by random sampling.

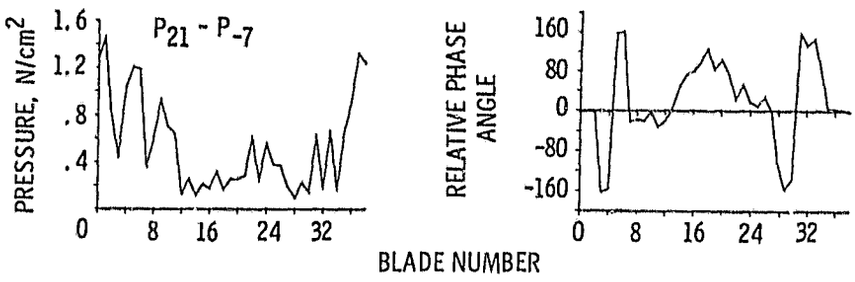

Figure 12. - Differential-pressure amplitude and phase distribution.